ORIGINAL ARTICLE   **Open Access**

Fermi-level flat band in a kagome magnet

T.Y. Yang[1†], Q. Wan[1†], J.P. Song[2], Z. Du[2], J. Tang[3], Z.W. Wang[4], N.C. Plumb[5], M. Radovic[5], G.W. Wang[6], G.Y. Wang[7], Z. Sun[8], Jia-Xin Yin[9], Z.H. Chen[10], Y.B. Huang[10], R. Yu[4], M. Shi[5], Y.M. Xiong[3,11*] and N. Xu[1,12*]

Abstract

The band structure in a kagome lattice can naturally exhibit flat band, Dirac cones, and van Hove singularity, enabling rich interplays between correlation and topology. However, the flat band is rarely detected just at the Fermi level in kagome materials, which would be crucial to realize emergent flat band physics. Here, combining angle-resolved photoemission spectroscopy, transport measurements and first-principles calculation, we observe a striking Fermi-level flat band in paramagnetic YCr_6Ge_6 as a typical signature of electronic kagome lattice. We explicitly unveil that orbital character plays an essential role to realize electronic kagome lattice in crystals with transition-metal kagome layers. We further engineer this material with magnetic rare earth elements to break the time-reversal symmetry of the Fermi-level kagome flat band. Our work establishes a Fermi-level flat band in a kagome magnet as an exciting quantum platform.

Keywords: Kagome lattice, Flat band, Band structure, Angle-resolved photoemission spectroscopy

1 Introduction

Due to the unique triangular-based corner sharing geometry, the kagome lattice (Fig. 1a) provides an exciting platform [1] for the realization of a series of unconventional quantum phases, including spin liquids [2], noncolinear magnetism [3], Chern energy gap [4], and unconventional charge ordering [5]. Particularly, the destructive quantum interference in the kagome lattice can lead to a flat band [6], which are proposed to host many emergent physics, such as the potential realization of high temperature fractional quantum Hall effect when a combination of spin-orbital coupling, time-reversal symmetry breaking and partial electron filling of the flat band is considered [7]. Along this direction, flat bands in several kagome materials have been successfully identified [8–17]. However, in those materials, the flat band is fairly far away from the Fermi level (usually on the order of 100 meV away from Fermi level), limiting its potential for further funda-

mental research and its application value in quantum devices.

In this paper, using angle-resolved photoemission spectroscopy (ARPES), we report the direct observations of typical kagome band structure with a Fermi-level flat band in paramagnet YCr_6Ge_6 (Fig. 1a), consisting with previous transport and first-principle calculation results [18]. We unveil that orbital character plays an important role in formation of flat band in kagome materials, with band flatness decomposed for $d_{x^2-y^2}/d_{xy}$ states. We further introduce ferromagnetism in the system by substitution Y with magnetic Gd, in which the Fermi-level flat band is preserved. Beside of systems with transition metals V [5, 16, 17, 19], Mn [3, 4, 15, 20–23], Fe [8, 10, 24, 25] and Co [9, 11–14, 26–28] kagome planes, Cr-based kagome magnet $(Y,Gd)Cr_6Ge_6$ provides a good platform to study the intrinsic properties of Fermi-level flat band, and its interplay with spin-orbit coupling (SOC) and time reversal symmetry breaking.

2 Results

2.1 Fermi-level flat band in YCr_6Ge_6

Firstly, we map the in-plane band structure with $h\nu$ = 55 eV, corresponding to the k_z = 0 plane in the bulk Brillouin

*Correspondence: yxiong@ahu.edu.cn; nxu@whu.edu.cn
[3]Department of Physics, School of Physics and Optoelectronics Engineering, Anhui University, Hefei 230601, China
[1]Institute for Advanced Studies, Wuhan University, Wuhan 430072, China
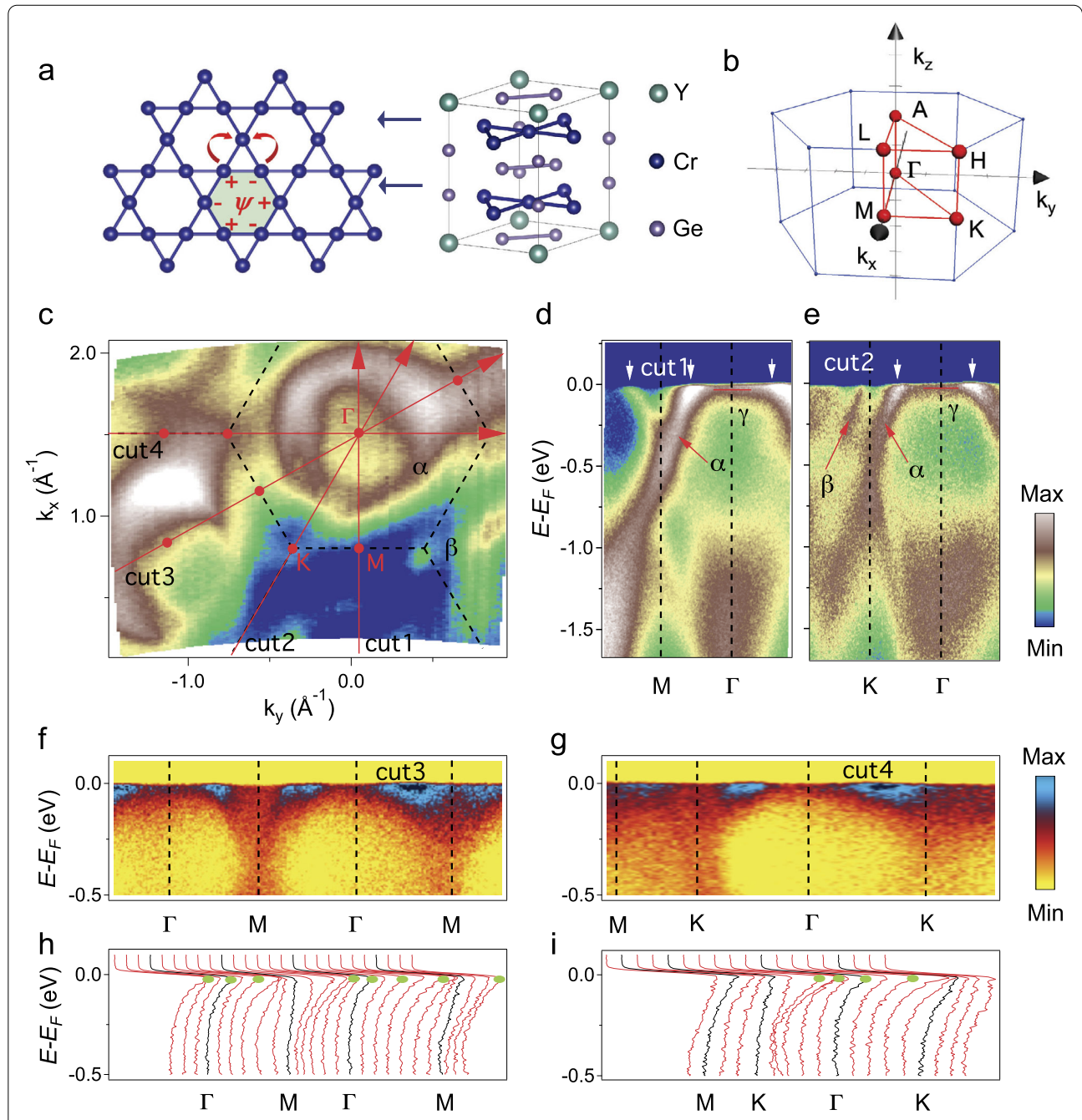Full list of author information is available at the end of the article †Equal contributors

Figure 1 Crystal and electronic structures of YCr$_6$Ge$_6$. (**a**) Crystal structure of YCr$_6$Ge$_6$, with Cr-kagome planes in a non-distorted stacking form. (**b**) Bulk Brillouin zone with the high-symmetry points indicated. (**c**) Photoemission intensity plot at E_F in the $k_z = 0$ plane. (**d**)–(**e**) Photoemission intensity plot along the Γ-M and Γ-K directions, with the momentum path indicated as cut1 and cut2 in (**c**), respectively. (**f**)–(**g**) Photoemission intensity along the cut3 and cut4 directions. (**h**)–(**i**) Corresponding EDC plots along the cut3 and cut4 direction in (**c**), with the flat band peak marked
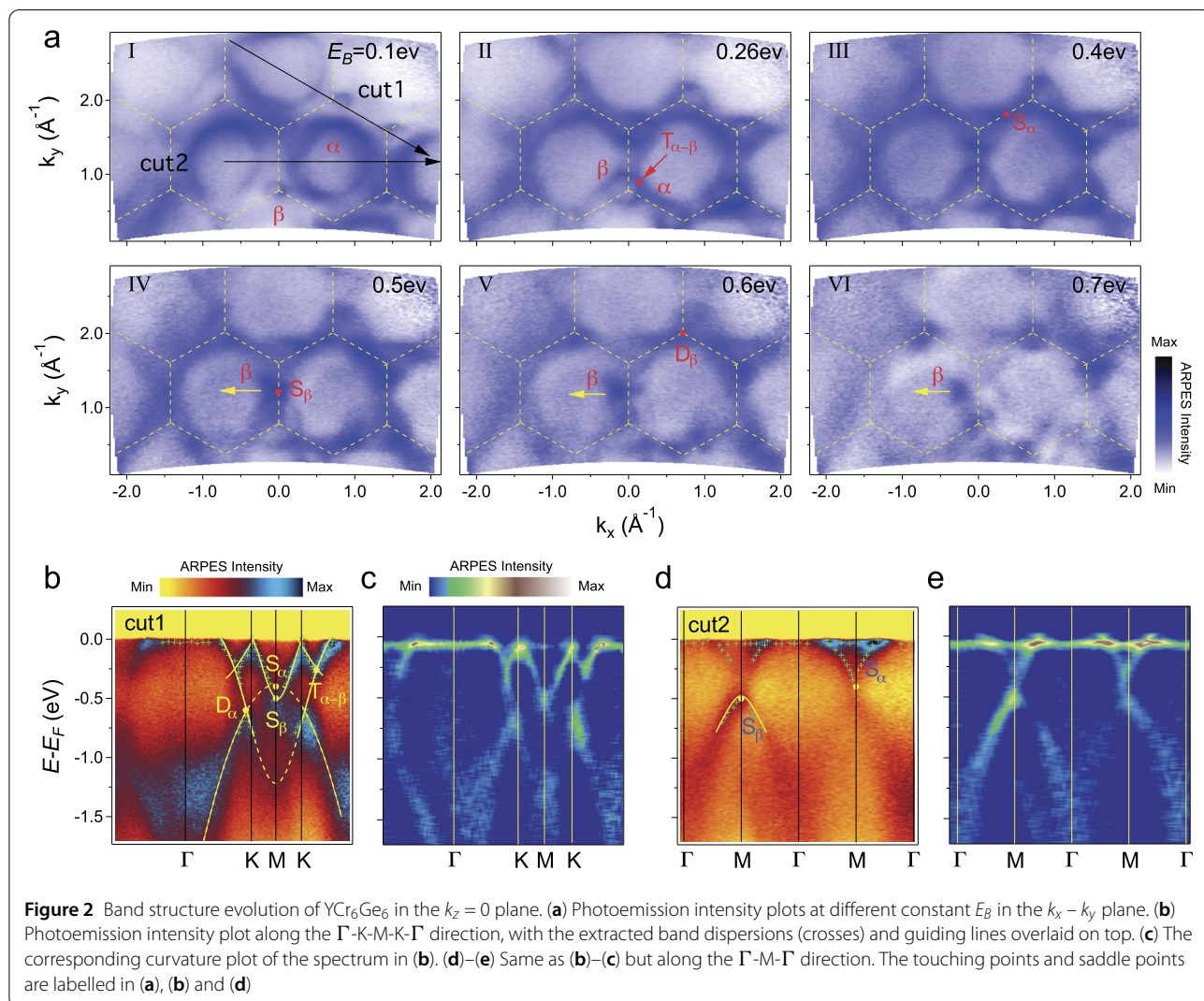
zone (BZ) (Fig. 1b). The Fermi surface (FS) consists of a big pocket (named as α) centered at the Γ point, and a hot spot (labeled as β) at the K point (Fig. 1c). The α band crosses Fermi energy (E_F) along the Γ-M (Fig. 1d) and Γ-K (Fig. 1e) directions, with Fermi momentum indicated by
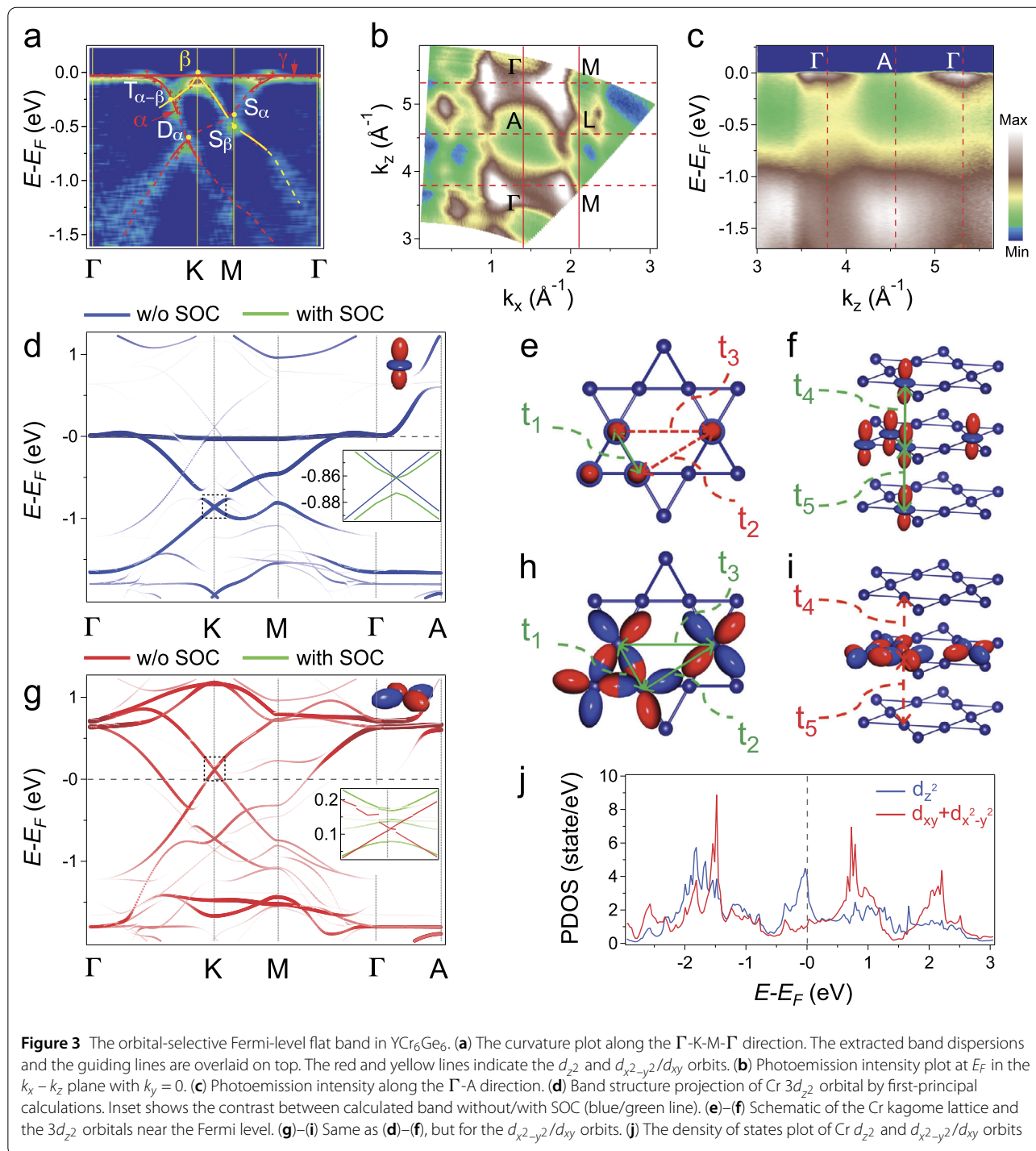
arrows. Interestingly, additional flat band, named as γ, is clearly observed near E_F. We note spectra weight of the α and flat γ bands in the first BZ are much less intense than that from higher BZs (Fig. 1c-e), due to the matrix element effect of photoemission. To eliminate the strong

intensity variation and focus on the band dispersion, we plot the experimental results along the Γ-M direction in the 2nd BZ, with the ARPES intensity and energy distribution curve (EDC) plotted in Fig. 1f and h, respectively. The flat band γ clearly appears with peaks near E_F in EDC plot along the Γ-M direction between two 2nd Γ points. Similarly, the flat band γ is explicitly observed near E_F along the Γ-K-M direction in higher BZs as seen from results shown in Fig. 1g and i. In addition to the high-symmetry directions, the γ band shows no dispersion at E_F in whole the $k_z = 0$ plane (see Additional file 1 Fig. S3), indicating an electronic kagome lattice origin of the Fermi-level flat band γ.

Besides flat band, YCr$_6$Ge$_6$ shows complete hallmarks of electronic kagome lattice including Dirac dispersions and saddle points. Figure 2a shows band structure evolution in the $k_z = 0$ plane. From E_F (Fig. 1c) to higher E_B (Fig. 2a-I), the hole-like α pocket at the Γ points also becomes bigger

and the β band at K point evolves from a single hot spot to a circular pocket. Further to higher E_B (Fig. 2a-II), the α and β pockets further expand and touch each other at $T_{\alpha-\beta}$ point along the Γ-K direction at $E_B \sim 0.26$ eV. Then the α and β pockets become even bigger at higher E_B, and the two α bands touch each other at the saddle point S_α along the Γ-M direction at $E_B \sim 0.4$ eV (Fig. 2a-III). At E_B higher than the S_α point, the α band evolves from big hole-like pockets around different Γ points to small electron-like pockets around the K point. Then two β bands touch each other at the saddle point S_β along the M-K direction at $E_B = 0.5$ eV (Fig. 2a-IV). The β band evolves from six small hole-like pockets at different K points to single big electron-like pockets centered at the Γ point as $E_B > 0.5$ eV, that becomes smaller and moves towards to the center of BZ with higher E_B, as seen from Fig. 2a-IV-VI. Furthermore, the electron-like α pocket at the K point shrinks into a single point D_α at $E_B \sim 0.6$ eV (Fig. 2a-V), and become

Figure 2 Band structure evolution of YCr$_6$Ge$_6$ in the $k_z = 0$ plane. (**a**) Photoemission intensity plots at different constant E_B in the $k_x - k_y$ plane. (**b**) Photoemission intensity plot along the Γ-K-M-K-Γ direction, with the extracted band dispersions (crosses) and guiding lines overlaid on top. (**c**) The corresponding curvature plot of the spectrum in (**b**). (**d**)–(**e**) Same as (**b**)–(**c**) but along the Γ-M-Γ direction. The touching points and saddle points are labelled in (**a**), (**b**) and (**d**)

Figure 3 The orbital-selective Fermi-level flat band in YCr$_6$Ge$_6$. (**a**) The curvature plot along the Γ-K-M-Γ direction. The extracted band dispersions and the guiding lines are overlaid on top. The red and yellow lines indicate the d_{z^2} and $d_{x^2-y^2}/d_{xy}$ orbits. (**b**) Photoemission intensity plot at E_F in the $k_x - k_z$ plane with $k_y = 0$. (**c**) Photoemission intensity along the Γ-A direction. (**d**) Band structure projection of Cr $3d_{z^2}$ orbital by first-principal calculations. Inset shows the contrast between calculated band without/with SOC (blue/green line). (**e**)–(**f**) Schematic of the Cr kagome lattice and the $3d_{z^2}$ orbitals near the Fermi level. (**g**)–(**i**) Same as (**d**)–(**f**), but for the $d_{x^2-y^2}/d_{xy}$ orbits. (**j**) The density of states plot of Cr d_{z^2} and $d_{x^2-y^2}/d_{xy}$ orbits

a hole-like pockets at higher E_B (Fig. 2a-VI). The touching point $T_{\alpha-\beta}$, Dirac point D_α and saddle points S_α and S_β are clearly resolved in the intensity and curvature plots along the Γ-K-M and Γ-M directions in Fig. 2b-e. The effective masses m^* of the α and β bands change the sign along the Γ-K-M and Γ-M directions at the S_α and S_β points, respectively.

2.2 Orbit-selectivity in formation of flat band

Our photon energy dependent ARPES measurements in Fig. 3b further indicate that inter-kagome-layers interaction is non-negligible in YCr$_6$Ge$_6$. The periodical variation along the k_z direction is a direct evidence of the bulk electronic states origins for the ARPES signals. We note that the periodicity along k_z is of $4\pi/c$, as twice as that in

the bulk BZ along the k_z direction ($2\pi/c$), because the two Cr kagome lattice in the unite cell are crystalline equivalence (Fig. 1a). Along the out of plane direction Γ-A-Γ (Fig. 3c), ARPES intensity near E_F only appears near the Γ point, corresponding to the flat band γ closed to E_F in the $k_z = 0$ plane. The photon energy dependent ARPES results demonstrate a planar flat band nature of γ, which is nondispersive feature in the $k_z = 0$ plane, indeed dispersive along the k_z direction.

Our first-principal calculations projected on Cr-3d_{z^2} orbit (Fig. 3d) show a good agreement with the observed α and γ bands (Fig. 3a). Our calculations further suggest that the observed β band corresponds the lower branches of the Dirac dispersion for the Cr-3$d_{x^2-y^2}$ and 3d_{xy} states (Fig. 3g). As seen from the insets of Fig. 3d and g, SOC opens gaps around 10 and 30 meV for the Dirac points at the K point for the d_{z^2} and $d_{x^2-y^2}/d_{xy}$ states, respectively. We note that a renormalization fact of 1.6 is needed for the calculation results to fit the overall features of experimental results (Additional file 1 Fig. S4), indicating a moderate electronic correlation effect in YCr$_6$Ge$_6$.

The unique behavior of the planar Fermi-level flat band γ is related to the intrinsic orbital character for the layered kagome lattice. As seen from Fig. 3e, intra-kagome-plane hopping process of the d_{z^2} electrons is dominated by t_1 and other in-plane hopping terms (t_2 and t_3) are negligibly weak. Therefore, both the d_{z^2} bands in the $k_z = 0$ plane (Fig. 3a and d) show a typical 2D electronic kagome lattice with Fermi-level flat band, von Hove singularity and Dirac dispersion. The hopping of d_{z^2} electrons between the adjacent kagome planes (t_4 and t_5 in Fig. 3f) are considerable, as intermediated by the spacing layers (Fig. 1a). The inter layer hoping terms lead to promising k_z dispersion of the planar Fermi-level flat band. The abnormal transport anisotropy in YCr$_6$Ge$_6$ ([18] and Additional file 1 Fig. S7), with the in-plane resistivity more than twice larger than the out-of-plane one, provides transport signatures of the planar flat band. The planar Fermi-level flat band also leads to a peak in density of states (DOS) at E_F (Fig. 3j). The relatively big Sommerfeld coefficient (80.5 mJ K^{-2} mol^{-1}) experimentally determined by heat capacity measurements serves as another transport property supporting the planar flat band.

Distinct from the d_{z^2} electrons, the inter-layer interaction of $d_{x^2-y^2}$ and d_{xy} orbits are expected to be weak (Fig. 3i), which results in less dispersive feature along the Γ-A direction (Fig. 3g). In the meantime, the $d_{x^2-y^2}$ and d_{xy} orbits lay in the kagome plane and can induce additional in-plane hopping between the second and third nearest-neighbour sites (Fig. 3h), respectively. The additional terms t_2 and t_3 terms destroy the flatness of the $d_{x^2-y^2}$ and d_{xy} orbits locating at about 0.7 eV above E_F.

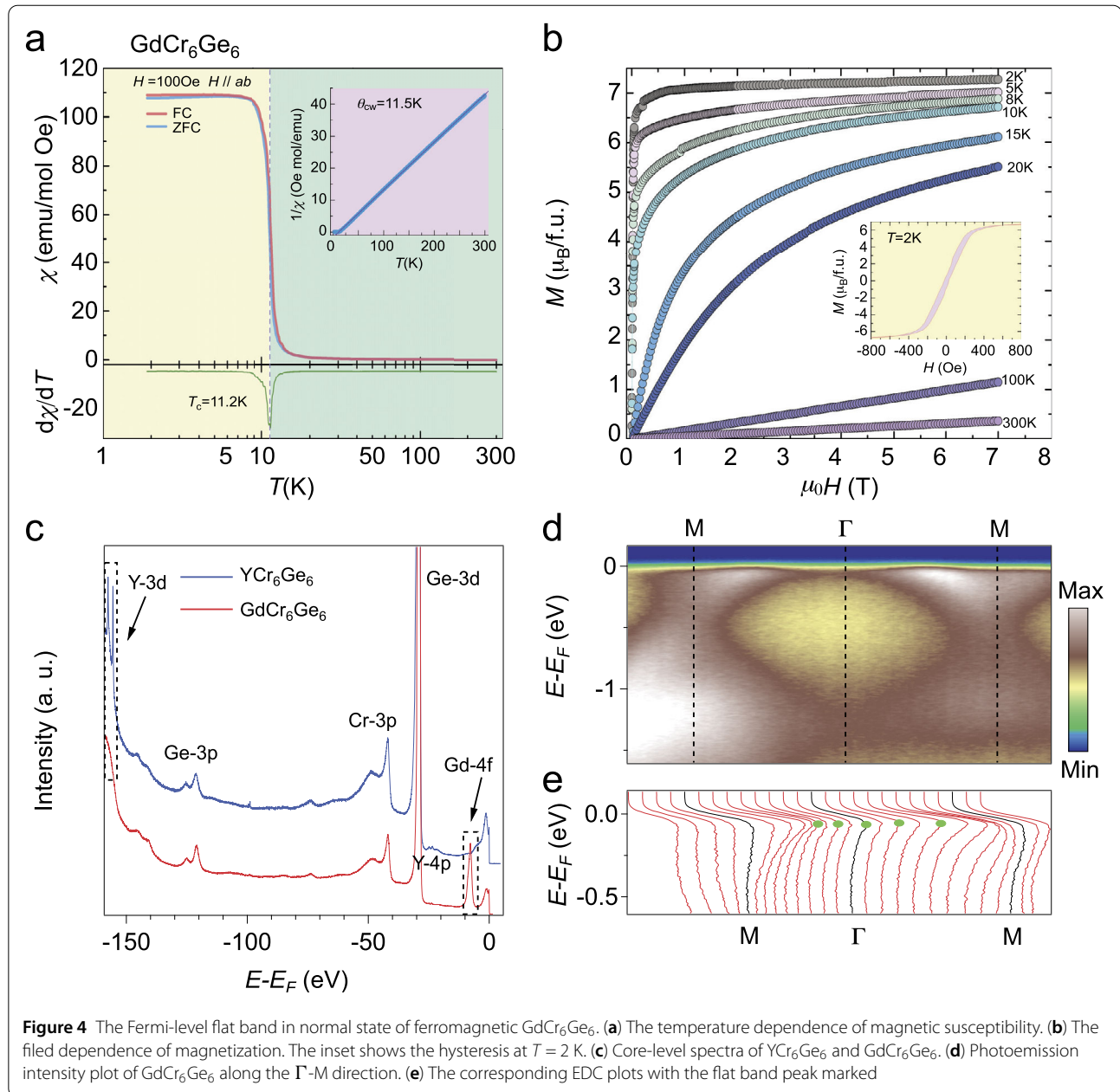### 2.3 Ferromagnetism and Fermi-level flat band in GdCr$_6$Ge$_6$

We further systematically engineer this kagome metal with magnetic rare earth element Gd to break time-reversal symmetry of the Fermi-level flat band. The temperature dependent magnetic susceptibility measurements on GdCr$_6$Ge$_6$ reveals the emergence of ferromagnetic ordering below a Curie temperature $T_C \sim 11.2$ K, which is consistent to the Weiss temperature $\theta_{CW} \sim 11.5$ K extracted from the data of paramagnetic phase (Fig. 4a). The magnetization M shows saturation and hysteresis below T_C (Fig. 4b), further confirmed the ferromagnetism. Since Gd 4f shell is half filled, there is a large local moment in Gd. Therefore, the ferromagnetism could mainly arise from the localized 4f electrons in Gd, which is away from Fermi-level. The core-level spectra of YCr$_6$Ge$_6$ and GdCr$_6$Ge$_6$ are shown in Fig. 4c, with Gd-4f peaks at $E_B \sim 8$ eV and Y-3d one at $E_B \sim 155$ eV, respectively. The band structure of GdCr$_6$Ge$_6$ (Fig. 4d) is very similar as that of YCr$_6$Ge$_6$ (Fig. 2d), with the Fermi-level flat band preserved in GdCr$_6$Ge$_6$ above T_C. Time reversal symmetry breaking and SOC are expected to split the spin degeneracy of the flat band γ and separate it from the α band by opening a gap at the Γ point, which can induce a topological Chern band in ferromagnetic phase of GdCr$_6$Ge$_6$. In future, we hope to further resolve the magnetic splitting of the flat band through high resolution and ultra-low temperature ARPES, and explore the tantalizing unusual anomalous transverse transports as well as the quantization properties of the magnetic flat band [7, 29]. For partially substituted compounds, the susceptibilities and ARPES results also present similar magnetic properties and the Fermi-level flat band in electronic structure, as shown in Fig. S8 of Additional file 1.

3 Conclusion and discussion

We directly observed a Fermi-level flat band from Cr-d_{z^2} electrons in paramagnetic YCr$_6$Ge$_6$ and normal state of ferromagnetic GdCr$_6$Ge$_6$, together with other signatures of typical kagome lattice band structure e.g. von Hove singularity and Dirac dispersions. The Fermi-level flat band can explain the abnormal behaviours in transport measurements. Our results demonstrate that orbital character plays an essential role for realization of flat band in transition metal kagome layers. Topological Chern band are expected in the ferromagnetic state of GdCr$_6$Ge$_6$. The Cr-based kagome magnets (Y,Gd)Cr$_6$Ge$_6$ provide a novel platform for investigating Fermi-level flat band, and its interplay with time-reversal symmetry breaking and SOC.

4 Method

High-quality (Y,Gd)Cr$_6$Ge$_6$ single crystals were grown by the flux method using tin as a flux. The starting elements mixture was heated to 1100°C over 8 h, kept at

Figure 4 The Fermi-level flat band in normal state of ferromagnetic $GdCr_6Ge_6$. (**a**) The temperature dependence of magnetic susceptibility. (**b**) The filed dependence of magnetization. The inset shows the hysteresis at T = 2 K. (**c**) Core-level spectra of YCr_6Ge_6 and $GdCr_6Ge_6$. (**d**) Photoemission intensity plot of $GdCr_6Ge_6$ along the Γ-M direction. (**e**) The corresponding EDC plots with the flat band peak marked

1100°C for 10 h and then slowly cooled to 600°C at the rate of 3°C/h, and finally decanted in a centrifuge. ARPES measurements were performed on the "surface and interface" beamline of the Swiss Light Source and "Dreamline" beamline of the Shanghai Synchrotron Radiation Facility, with an overall energy resolution of the order of 20 meV, angular resolution of 0.1°, at T = 20 K. The electronic structure of YCr_6Ge_6 was calculated based on the density functional theory and the local density approximation for the exchange correlation potential, as implemented in the plane-wave pseudopotential based Vienna ab initio simulation package. The wave functions were ex-

panded in plane waves with a cutoff energy of 470 eV and Monkhorst–Pack k points were 9 × 9 × 5. The residual forces are less than 0.01 eV/Å and SOC is included by using the second-order variational procedure.

Supplementary information

Additional file 1. Supplementary information (PDF 6.8 MB)

Availability of data and materials

The data and materials that support the findings of this study are available from the corresponding author upon reasonable request.

Declarations

Competing interests

The authors declare no competing interests.

Author contribution

NX and YX supervise the project. TY, QW, and NX did the ARPES experiments with the help of NP, MR, JY, ZC, YH and MS. JS, ZD, YW, JT, GW, GW, ZS and YX grow the materials and performed transport measurements. ZW and RY did calculations. All authors read and approved the final manuscript.

Author details

[1] Institute for Advanced Studies, Wuhan University, Wuhan 430072, China. [2] Anhui Province Key Laboratory of Condensed Matter Physics at Extreme Conditions, High Magnetic Field Laboratory, Chinese Academy of Sciences, Hefei 230031, China. [3] Department of Physics, School of Physics and Optoelectronics Engineering, Anhui University, Hefei 230601, China. [4] School of Physics and Technology, Wuhan University, Wuhan 430072, China. [5] Swiss Light Source, Paul Scherrer Institut, CH-5232 Villigen PSI, Switzerland. [6] Analytical and Testing Center, Chongqing University, Chongqing 401331, China. [7] Chongqing Institute of Green and Intelligent Technology, Chinese Academy of Sciences, Chongqing 400714, China. [8] National Synchrotron Radiation Laboratory, University of Science and Technology of China, Hefei, Anhui 230029, China. [9] Laboratory for Quantum Emergence, Department of Physics, Southern University of Science and Technology, Shenzhen, Guangdong 518055, China. [10] Shanghai Synchrotron Radiation Facility, Shanghai Advanced Research Institute, Chinese Academy of Sciences, Shanghai 201204, China. [11] Hefei National Laboratory, Hefei 230028, China. [12] Wuhan Institute of Quantum Technology, Wuhan 430206, China.

Publisher's Note

Springer Nature remains neutral with regard to jurisdictional claims in published maps and institutional affiliations.

References

1. Syôzi I (1951) Statistics of kagomé lattice. Prog Theor Phys 6:306–308
2. Broholm C, Cava RJ, Kivelson SA, Nocera DG, Norman MR, Senthil T (2020) Quantum spin liquids. Science 367:0668
3. Tomiyoshi S, Yamaguchi Y (1982) Magnetic structure and weak ferromagnetism of Mn_3Sn studied by polarized neutron diffraction. J Phys Soc Jpn 51:2478–2486
4. Yin JX, Ma W, Cochran TA, Xu X, Zhang SS, Tien HJ, Shumiya N, Cheng G, Jiang K, Lian B, Song Z, Chang G, Belopolski I, Multer D, Litskevich M, Cheng ZJ, Yang XP, Swidler B, Zhou H, Lin H, Neupert T, Wang Z, Yao N, Chang TR, Jia S, Hasan MZ (2020) Quantum-limit Chern topological magnetism in $TbMn_6Sn_6$. Nature 583:533–536
5. Neupert T, Denner MM, Yin JX, Thomale R, Hasan MZ (2022) Charge order and superconductivity in kagome materials. Nat Phys 18:137–143
6. Mielke A (1991) Ferromagnetic ground states for the Hubbard model on line graphs. J Phys A, Math Gen 24:L73
7. Tang E, Mei JW, Wen XG (2011) High-temperature fractional quantum Hall states. Phys Rev Lett 106:236802
8. Lin Z, Choi JH, Zhang Q, Qin W, Yi S, Wang P, Li L, Wang Y, Zhang H, Sun Z, Wei L, Zhang S, Guo T, Lu Q, Cho JH, Zeng C, Zhang Z (2018) Flatbands and emergent ferromagnetic ordering in Fe_3Sn_2 kagome. Phys Rev Lett 121:96401
9. Yin JX, Zhang SS, Chang G, Wang Q, Tsirkin SS, Guguchia Z, Lian B, Zhou H, Jiang K, Belopolski I, Shumiya N, Multer D, Litskevich M, Cochran TA, Lin H, Wang Z, Neupert T, Jia S, Lei H, Hasan MZ (2019) Negative flat band magnetism in a spin–orbit-coupled correlated kagome magnet. Nat Phys 15:443–448
10. Kang M, Ye L, Fang S, You JS, Levitan A, Han M, Facio JI, Jozwiak C, Bostwick A, Rotenberg E, Chan MK, McDonald RD, Graf D, Kaznatcheev K, Vescovo E, Bell DC, von Kaxiras E, den Brink J, Richter M, Ghimire MP, Checkelsky JG, Comin R (2020) Dirac fermions and flat bands in the ideal kagome metal FeSn. Nat Mater 19:163–169
11. Liu Z, Li M, Wang Q, Wang G, Wen C, Jiang K, Lu X, Yan S, Huang Y, Shen D, Yin JX, Wang Z, Yin Z, Lei H, Wang S (2020) Orbital-selective Dirac fermions and extremely flat bands in frustrated kagome-lattice metal CoSn. Nat Commun 11:4002
12. Yin JX, Shumiya N, Mardanya S, Wang Q, Zhang SS, Tien HJ, Multer D, Jiang Y, Cheng G, Yao N, Wu S, Wu D, Deng L, Ye Z, He R, Chang G, Liu Z, Jiang K, Wang Z, Neupert T, Agarwal A, Chang TR, Chu CW, Lei H, Hasan MZ (2020) Fermion–boson many-body interplay in a frustrated kagome paramagnet. Nat Commun 11:4003
13. Kang M, Fang S, Ye L, Po HC, Denlinger J, Jozwiak C, Bostwick A, Rotenberg E, Kaxiras E, Checkelsky JG, Comin R (2020) Topological flat bands in frustrated kagome lattice CoSn. Nat Commun 11:4004
14. Meier WR, Du MH, Okamoto S, Mohanta N, May AF, McGuire MA, Bridges CA, Samolyuk GD, Sales BC (2020) Flat bands in the CoSn-type compounds. Phys Rev B 102:075148
15. Li M, Wang Q, Wang G, Yuan Z, Song W, Lou R, Liu Z, Huang Y, Liu Z, Lei H, Yin Z, Wang S (2021) Dirac cone, flat band and saddle point in kagome magnet YMn_6Sn_6. Nat Commun 12:3129
16. Hu Y, Teicher SML, Ortiz BR, Luo Y, Peng S, Huai L, Ma J, Plumb NC, Wilson SD, He J, Shi M (2022) Topological surface states and flat bands in the kagome superconductor CsV_3Sb_5. Sci Bull 67:495–500
17. Peng S, Han Y, Pokharel G, Shen J, Li Z, Hashimoto M, Lu D, Ortiz BR, Luo Y, Li H, Guo M, Wang B, Cui S, Sun Z, Qiao Z, Wilson SD, He J (2021) Realizing kagome band structure in two-dimensional kagome surface states of RV_6Sn_6 (R = Gd, Ho). Phys Rev Lett 127:266401
18. Ishii Y, Harima H, Okamoto Y, Yamaura JI, Hiroi Z (2013) YCr6Ge6 as a candidate compound for a kagome metal. J Phys Soc Jpn 82:023705
19. Ortiz BR, Gomes LC, Morey JR, Winiarski M, Bordelon M, Mangum JS, Oswald IWH, Rodriguez-Rivera JA, Neilson JR, Wilson SD, Ertekin E, McQueen TM, Toberer ES (2019) New kagome prototype materials: discovery of KV3Sb5, RbV_3Sb_5, and CsV_3Sb_5. Phys Rev Mater 3:094407
20. Nakatsuji S, Kiyohara N, Higo T (2015) Large anomalous Hall effect in a non-collinear antiferromagnet at room temperature. Nature 527:212–215
21. Nayak AK, Fischer JE, Sun Y, Yan B, Karel J, Komarek AC, Shekhar C, Kumar N, Schnelle W, Kübler J, Felser C, Parkin SSP (2016) Large anomalous Hall effect driven by a nonvanishing Berry curvature in the noncolinear antiferromagnet Mn3Ge. Sci Adv 2:e1501870
22. Kuroda K, Tomita T, Suzuki MT, Bareille C, Nugroho AA, Goswami P, Ochi M, Ikhlas M, Nakayama M, Akebi S, Noguchi R, Ishii R, Inami N, Ono K, Kumigashira H, Varykhalov A, Muro T, Koretsune T, Arita R, Shin S, Kondo T, Nakatsuji S (2017) Evidence for magnetic Weyl fermions in a correlated metal. Nat Mater 16:1090–1095
23. Liu ZQ, Chen H, Wang JM, Liu JH, Wang K, Feng ZX, Yan H, Wang XR, Jiang CB, Coey JMD, MacDonald AH (2018) Electrical switching of the topological anomalous Hall effect in a non-collinear antiferromagnet above room temperature. Nat Electron 1:172–177
24. Wang Q, Sun S, Zhang X, Pang F, Lei H (2016) Anomalous Hall effect in a ferromagnetic Fe_3Sn_2 single crystal with a geometrically frustrated Fe bilayer kagome lattice. Phys Rev B 94:075135
25. Ye L, Kang M, Liu J, von Cube F, Wicker CR, Suzuki T, Jozwiak C, Bostwick A, Rotenberg E, Bell DC, Fu L, Comin R, Checkelsky JG (2018) Massive Dirac fermions in a ferromagnetic kagome metal. Nature 555:638–642
26. Yin JX, Zhang SS, Li H, Jiang K, Chang G, Zhang B, Lian B, Xiang C, Belopolski I, Zheng H, Cochran TA, Xu SY, Bian G, Liu K, Chang TR, Lin H, Lu ZY, Wang Z, Jia S, Wang W, Hasan MZ (2018) Giant and anisotropic many-body spin–orbit tunability in a strongly correlated kagome magnet. Nature 562:91–95

27. Liu E, Sun Y, Kumar N, Muechler L, Sun A, Jiao L, Yang SY, Liu D, Liang A, Xu Q, Kroder J, Süß V, Borrmann H, Shekhar C, Wang Z, Xi C, Wang W, Schnelle W, Wirth S, Chen Y, Goennenwein STB, Felser C (2018) Giant anomalous Hall effect in a ferromagnetic kagome-lattice semimetal. Nat Phys 14:1125–1131
28. Wang Q, Xu Y, Lou R, Liu Z, Li M, Huang Y, Shen D, Weng H, Wang S, Lei H (2018) Large intrinsic anomalous Hall effect in half-metallic ferromagnet $Co_3Sn_2S_2$ with magnetic Weyl fermions. Nat Commun 9:3681
29. Rhim JW, Kim K, Yang BJ (2020) Quantum distance and anomalous Landau levels of flat bands. Nature 584:59–63